A Materials Approach to Resistive Switching Memory Oxides

M. Hasan, R. Dong, D. S. Lee, D. J. Seong, H. J. Choi, M.B. Pyun, and H. Hwang

***Abstract*—Several oxides have recently been reported to have resistance-switching characteristics for nonvolatile memory (NVM) applications. Both binary and ternary oxides demonstrated great potential as resistive-switching memory elements. However, the switching mechanisms have not yet been clearly understood, and the uniformity and reproducibility of devices have not been sufficient for gigabit-NVM applications. The primary requirements for oxides in memory applications are scalability, fast switching speed, good memory retention, a reasonable resistive window, and constant working voltage. In this paper, we discuss several materials that are resistive-switching elements and also focus on their switching mechanisms. We evaluated non-stoichiometric polycrystalline oxides (Nb_2O_5, and ZrO_x) and subsequently the resistive switching of Cu_xO and heavily Cu-doped MoO_x film for their compatibility with modern transistor-process cycles. Single-crystalline Nb-doped $SrTiO_3$ (NbSTO) was also investigated, and we found a Pt/single-crystal NbSTO Schottky junction had excellent memory characteristics. Epitaxial NbSTO film was grown on an Si substrate using conducting TiN as a buffer layer to introduce single-crystal NbSTO into the CMOS process and preserve its excellent electrical characteristics.**

***Index Terms*—ReRAM switching, binary and ternary oxides, oxygen vacancy, crystallinity, stoichiometry**

Manuscript received Feb. 27, 2008; revised Mar. 7, 2008.
Department of Materials Science and Engineering, Gwangju Institute of Science and Technology, #1, Oryong-dong, Buk-ku, Gwangju, 500-712, Korea
E-mail : hwanghs@gist.ac.kr

I. INTRODUCTION

The semiconductor industry is encountering both technological and fundamental challenges as device features are approaching the sub-100-nm regime. The increasing demand for device scaling, as clearly described by the International Technology Roadmap for Semiconductors (ITRS) [1], is a major issue. To overcome the limitations of conventional semiconductor devices, which are based on charge storage, various new nonvolatile-memory (NVM) devices such as phase-change, polymer, magnetic, and resistance RAMs (ReRAMs) have been investigated.

Of these novel NVMs, materials with reversible resistance switching at room temperature have become increasingly more attractive for today's semiconductor technology processes due to their drastically reduced power consumption, fast switching speed, and nondestructive readouts. Resistance-switching behaviors have been observed in metal–insulator–metal (MIM) memory cells. A reasonable compliance current should generally be set before resistance switching between a conductive ON and a less conductive OFF state is carried out. Applied compliance current has been suggested to not only control the initial electroforming step (so-called soft-breakdown) in the virgin sample, but also limit the excessive Joule-heating effect in the resistive-switching process that follows.

Up to now, two basic resistive-switching schemes, unipolar and bipolar switching, have been reported. If the resistive-switching procedure does not depend on the polarity of the applied voltage, it is called unipolar switching. This means that a high-resistance state (HRS) can be switched to a low-resistance state (LRS) using a voltage V_{Set} ($V_{Set} > V_{th}$, V_{th}: threshold voltage), and a

relatively lower voltage V_{Reset} ($V_{Reset} < V_{Set}$) can switch the LRS back to HRS. Bipolar switching is defined as HRS and LRS depending on switching polarity, i.e., V_{Set} and V_{Reset} have opposite polarities.

Various models have been proposed to explain the resistance-switching mechanism [2–19]. Actually, numerous materials in an MIM configuration had been reported as early as the 1960s that demonstrated hysteretic resistance switching. The present reinterest not only expands the sorts of switching materials available but also extends our understanding of the switching mechanism. Two physical mechanisms have been proposed. The first was by Liu et al. [2] who argued between the bulk or interface effect where polarized clusters were rearranged and the second was by Baikalov et al. [5] who proposed field-induced electrochemical migration. Subsequently, "three domains theory" was proposed by Rozenberg et al. [7], which is formed in between the top and bottom electrodes and the middle domain was suggested as a resistance-controlling layer.

Furthermore, the Schottky-barrier effect between the metal (oxide) top electrode and insulator was regarded as the origin of resistive switching according to Sawa et al. [8]. Therefore, the very thin interface layer, i.e., of only a few nanometers, is responsible for rectifying resistive switching. If the model of a P-type ($Pr_{0.7}Ca_{0.3}MnO_3$) Schottky contact is considered, the barrier height increases with the decreasing work function of the top electrode. Fujii et al. [9] further studied the rectifying *I-V* characteristics between an N-type ($SrTi_{0.99}Nb_{0.01}O_3$, NbSTO) oxide and a deep-work-function oxide ($SrRuO_3$, SRO) where an N-type Schottky contact was formed. Choi et al. [14] demonstrated that reasonable endurance cycles and data retention could be expected for polycrystalline $SrTiO_x$ samples prepared by pulse-laser deposition. Tokunaga et al. [6] reported *I-V* and resistance switching at the interface between various metal electrodes and $La_{1-x}Sr_{1+x}MnO_4$ (x = 0-1.0) crystal. The resistance-switching ratio has been suggested to depend on the amount of hole doping (x), which means that switching properties can be controlled by the doping level. There are still arguments for the Schottky-barrier model, e.g., the effect of the metal-work function. The Schottky-contact model seems reasonable for Pt, Au, and Ag. However, for Ti and Ag, where almost the same work function has been reported, the difference in interface properties cannot be fully understood although band bending caused by barrier height (width) has been proposed.

Since most switching materials have been poly-crystalline oxide, defects and grain boundaries have been unavoidable. Therefore, the trap-controlled space charge limited current (SCLC), reported by Odagawa et al. [9], has also been applied to explain switching mechanisms. Ohmic behavior ($I \propto V$) corresponds to an unfilled trap region at a lower voltage and the current-voltage change in relation to second order ($I \propto V^2$) at a higher voltage for a trap-filled region. Not only perovskite $Pr_{0.7}Ca_{0.3}MnO_3$ (PCMO) but also binary oxide Cu_xO was demonstrated to be controlled by the SCLC process according to Chen et al. [12] and Dong et al. [16]. Pt/NiO/Pt capacitors were also suggested to exhibit conductivity switching where the formation and deformation of conducting filaments were responsible as reported by Seo et al. [3]. Oka et al. [6] and Kozuka et al. [11] proposed interface Mott transition as a switching mechanism.

More recently, oxygen ions migrating along formed "paths" under negative or positive voltage have attracted a great deal of attention. Oxygen ions and vacancy movements have been reported by Wakiya et al. [22], where negative oxygen ions (O^{2-}) and electrons move toward the positive electrode whereas oxygen vacancies (V_O^{2+}) move to the negative electrode. Bulk oxide contains both oxygen vacancies and interstitial defects whereas similar defects have also been observed near the interface due to mismatch. Defect sites are also created because of chemical reactions and plasma damage. Very recently, a ReRAM-switching mechanism based on redox reaction has been described for a Fe-O system [23]. The transformation of Fe_2O_3 oxide to Fe_3O_4 is responsible for the proposed change in resistance. A report by IBM Zurich presented by Janousch et al. [24] showed direct evidence of oxygen vacancies related to the conducting path, which were controlled by the Cr in Cr:STO crystal. A better understanding of the effect of the source of oxygen ions (reservoirs) and the formation of this path is required. Table 1 summarizes the reported physical mechanisms for ReRAM although no single proposed mechanism can fully or universally explain

resistance-switching behaviors.

Except for unsolved switching mechanisms, several obstacles need to be overcome to meet the requirements of actual gigabit-memory devices. The scalability of memory oxide materials is a serious issue as most materials exhibit different resistive-switching behaviors as the film thickness decreases. Process-integration and compatibility issues are also extremely important considering the current technology for silicon CMOSs. One very serious problem in ReRAM devices is non-uniform memory switching. Most of the available data has not reported device-to-device uniformity, which is necessary for commercial gigabit-memory devices. Localized switching characteristics usually require a formation process, which also causes non-uniform switching.

All these problems need to be solved or at least clearly understood. Single-crystal oxides usually have uniform switching but are very difficult to grow on silicon substrates. Therefore, polycrystalline oxides with better uniformity are required. Other electrical properties such as short pulse-width requirements and better data-retention properties up to a decade are also required for high-speed NVM devices.

Although the usefulness of resistance-switching memory oxides is clear, numerous obstacles still need to be overcome. In what follows, we will explore the use of several polycrystalline and epitaxial binary and ternary oxides as memory-switching materials.

Table 1. Reported physical mechanisms for ReRAMs

Samples	Research groups	Driving modes	*I-V* (transport mechanisms)	Mechanisms
Ag/PCMO/YBCO (Pt)	Houston	Bipolar		Oxygen diffusion
Au/Cr:SZ(T)O/SRO	IBM (Zurich)	Bipolar		
Ag/PCMO/Pt	Matsushita, AIST	Bipolar	Space Charge Limited Current (SCLC)	Trapping
TiN/Cu_xO/Cu	Spansion	Bipolar		
Ti/PCMO, SRO/Nb:STO Theory	AIST&CERC	Bipolar	Schottky	Charging and/or Mott transition
Au (Pt)/STO/Au (Pt)	Zurich	Bipolar	Tunneling	Oxygen diffusion
Pt/NiO(TiO_2)/Pt	Fujitsu	Unipolar		
Theory, Pt/NiO/Pt	Paris-Sud & AIST	Unipolar		Mott transition
Pt/NiO/Pt	Samsung	Unipolar		Oxygen diffusion
Pt/Nb:STO Pt/Cu:MoO_x W/Cu_xO/Cu	GIST	Bipolar	SCLC+ Schottky+ tunneling*	Trapping+ charging+ oxygen diffusion*

*: Depends on materials

II. Resistive Switching of Binary Oxides

1. Resistive Switching of ZrOx

Polycrystalline ZrO_2 was deposited on a highly-doped *p*-type silicon substrate in an RF sputtering system using a Zr target in an argon and oxygen mixture. The stoichiometry and composition of the ZrO_x films could be controlled by changing the deposition conditions, which modulated the electrical properties of the Pt/ZrO_x/p-Si structure. The non-stoichimetric ZrO_x films were deposited at 400 ℃ after standard cleaning of the *p*-type silicon wafer had been done. Post-deposition annealing was done in an oxygen ambient at 250 ℃ for 10 min to grow a thin stoichiometric oxide surface layer. A Pt/ZrO_x/p-Si device with 100-nm-thick platinum (Pt) gate electrode was fabricated by photolithography. The chemical-binding energy was analyzed using X-ray photoelectron spectroscopy (XPS). The current–voltage (*I–V*) characteristics of the samples were measured with an HP4155 semiconductor parameter analyzer.

Fig. 1 shows the high resolution transmission electron microscope (HR-TEM) image and the x-ray diffraction spectroscopy data (inset). Both confirm the crystalline structure of the film. Our analysis with Rutherford backscattering spectrometry (RBS) (not shown) suggested

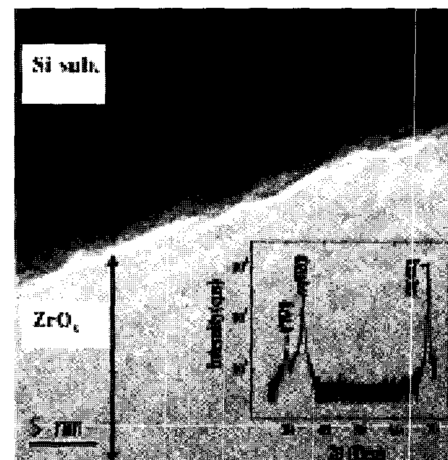

Fig. 1. HR-TEM image of crystalline ZrO_2 film grown at 400°C. Inset confirms both tetragonal and monoclinic phases.

that the average oxygen to zirconium ratio was 1.65. The X-ray diffraction (XRD) pattern shows that the ZrO_x film had a mixed structure with tetragonal (101) and monoclinic (020) planes.

XPS-depth profiling was undertaken (Fig. 2) to confirm the composition and binding energy, and based on this the ZrO_x film was found to be composed of three layers, i.e., "top", "transition", and "conducting-bulk". Two Zr $3d_{5/2}$ peaks (Zr at 179.04 eV and ZrO_2 at 183.2 eV) were observed, and the additional peak was related to Zr $3d_{3/2}$ for metallic Zr and ZrO_2 ($\Delta\sim$ 2.2 eV). The peak, which is associated with a ZrO_2 layer, indicated stoichiometric oxide layer, as shown in Fig. 2(a). However, the bulk and transition layers both had peaks from metallic Zr and ZrO_2, which indicate an excess-metal non-stoichiometric ZrO_2 layer. There is a schematic of all layers in Fig. 2 (d).

Stable unipolar resistance switching was observed with one order of magnitude of the resistance ratio plotted in Fig. 3 (a). The device was set to an ON state by applying a voltage of ~1.7 V and it could return to the OFF state at a voltage of ~1.2 V. An nMOSFET was also fabricated with a $Pt/ZrO_x/n^+$-Si structure on the source side. Figure 3 (b) plots the I_d-V_g characteristics where pulse stress was applied to change the resistance state. The stress time was 100 ns and the pulse amplitude was 6 V for the ON condition and 2 V for the OFF.

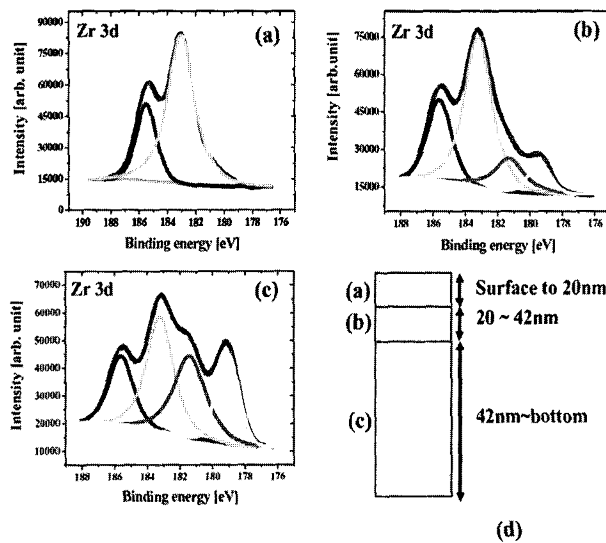

Fig. 2. XPS spectra of Zr 3d (a) top oxide: from top to 20 nm in depth, (b) transition region: from 20 to 42 nm, and (c) bulk region. (d) Schematic of structure of ZrO_x film in direction of depth.

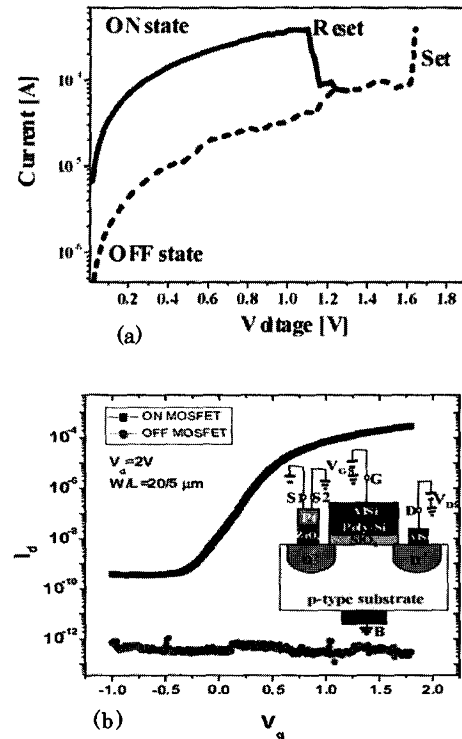

Fig. 3. (a) *I-V* characteristics of $Pt/ZrO_x/Si$ and (b) Id-Vg curve for nMOS transistor with ZrO_x as memory material.

We propose a possible model of switching for non-schotiometric ZrO_x based on these XPS data. As different layers have different compositions and metallic Zr content, they are expected to have different resistance values. Therefore, the top stoichiometric ZrO_2 layer has high resistivity, the transition region has medium resistivity, and the bulk layer is a conductor (Fig. 4).

Based on these facts, the following can be concluded. During the activation process (formation), the top oxide layer needs be broken (soft-breakdown) before resistance switching can be generated.

Bulk ZrO_x should be a good conductor, and the sheet resistance of as-deposited ZrO_x measured with both a four-point probe and Hall measurement were 12.4 Ω/□. Since the thickness of ZrO_x is about 120 nm and the device area is $9X10^{-6}\,cm^2$, the calculated bulk resistance of ZrO_x should thus be $2X10^{-4}$ Ω. However, based on the *I-V* curves in Fig. 3, the device resistance is about 1 to 10 kΩ. As the significant difference in the resistance value derives from the resistance of the transition layer and top oxide layer, high voltage should only be applied to the top insulating layer, which causes soft-breakdown during the initial forming stress condition. In addition, if

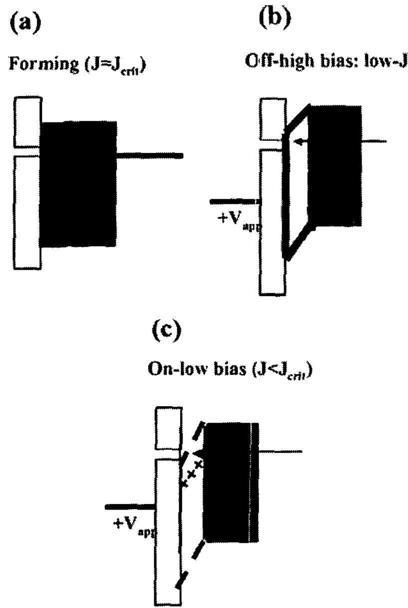

Fig. 4. Proposed resistive-switching mechanism of ZrO_x film: (a) Band diagram after formation, (b) high-resistance state without positive charge, and (c) low resistance state with positive charge.

the transition layer is considered to have excess Zr, high voltage stress will cause the metallic Zr to ionize and generate positive Zr ions, and the positive charges in ZrO_x will cause band bending which in turn will enhance current flow through the transition layer (Fig. 4(c)). If the applied bias is more than the critical value, electrons can be expected to accumulate at the transition layer due to the limited current flow in the top oxide layer. Furthermore, this might cause electrons to recombine with positive Zr ions, which in turn will reduce the electric field and current flow (Fig. 4(b)).

2. Resistive Switching of Nb_2O_5

Thin-film Nb_2O_5 diodes are unique insulators that have bistable switching and memory properties because of their low-voltage requirements (<1 V) for switching and also because switching is independent insulator thickness. We directly deposited a 58-nm-thick Nb_2O_5 film on a highly doped p-type Si (100) substrate using a PLD process in an oxygen ambient using a KrF excimer laser (248-nm wavelength, 30-ns pulse width, and operated at 1 Hz) after standard wafer cleaning had been done followed by HF-final cleaning to maintain a hydrogen-passivated silicon surface. The substrate

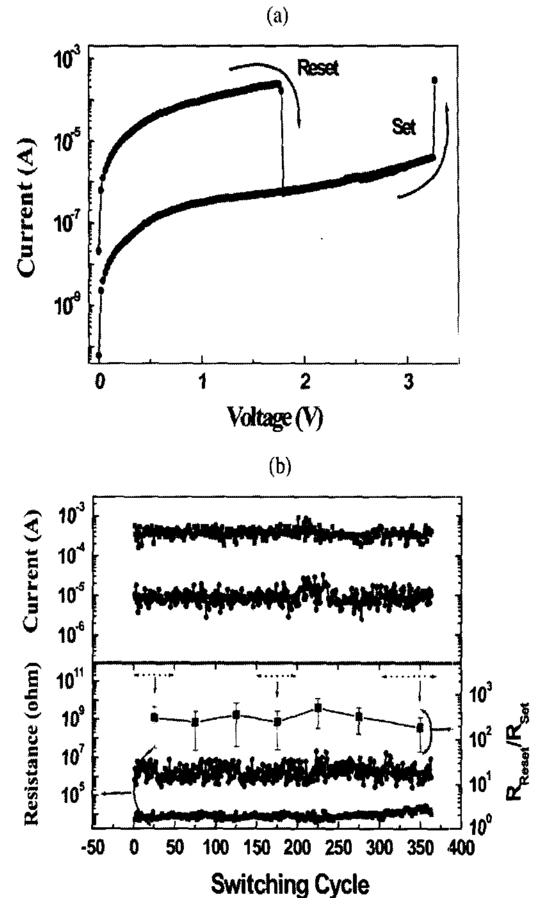

Fig. 5. (a) Current–voltage characteristics of high- and low-resistance states for $Pt/Nb_2O_5/Si$ device. (b) Reproducible resistance switching was demonstrated.

temperature was 700 ℃, and the oxygen partial pressure was 30 mtorr. Post-oxide annealing was carried out at 800 ℃ for 5 min in a nitrogen ambient at atmospheric pressure in a tube furnace to achieve crystallization after the Nb_2O_5 film had been deposited. An approximately 150-nm-thick platinum top electrode was deposited by RF-magnetron sputtering through a shadow mask with a $1.5X10^{-4}$ cm^2 electrode area. Rutherford backscattering spectroscopy (RBS) revealed that the ratio of Nb:O was approximately 0.4. The XRD pattern indicated that the film was polycrystalline after annealing at 800 ℃, and the as-deposited sample at 700 ℃ had no clear XRD peaks.

Fig. 5 (a) shows that HRS was switched to LRS, and that the transition was defined as "set". Moreover, the subsequent transition from LRS to HRS was defined as "reset". The reset and set voltages were approximately 2 and 3.5 V. Figure 5 (b) shows reproducible resistance-switching cycles, and the current compliance of the reset state was approximately 500 and that of the set state was

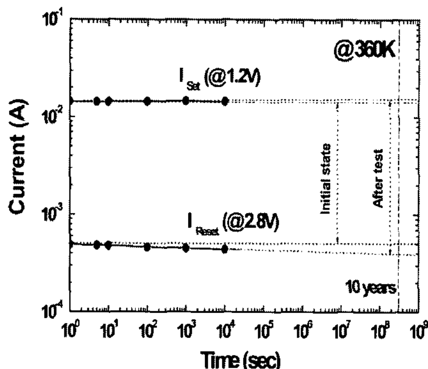

Fig. 6. Degradation in resistance ratio measured at 85℃. Estimated degradation in resistance ratio at 85℃ for 10 years is approximately 7 %.

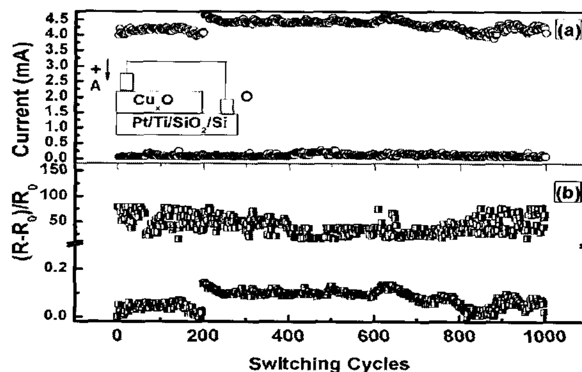

Fig. 7. (a) Current vs switching cycles for (M-Cu_xO-M) heterostructures. (b) Resistance changing ratio ($\Delta R/R_0=(R-R_0)/R_0$) vs switching cycles for M-Cu_xO-M heterostructures.

10 μA. The resistance ratios of LRS to HRS ranged from 50 to 100. Figure 6 plots the degradation in the resistance ratio at 85 ℃, and the estimated degradation in the resistance ratio at 85 ℃ for 10 years is approximately 7%, demonstrating Nb_2O_5 as a potential candidate for NVM applications.

III. Resistive Switching of Cu- and Mo-Based Oxides

1. Resistive Switching of CuxO

The Cu starting material in Metal-Cu_xO-Metal (M-Cu_xO-M) heterostructures is relatively inexpensive, non-toxic, abundantly available from the earth, and extensively used in modern semiconductor processes. Fabrication of the M-Cu_xO-M heterostructure is fully compatible with the standard CMOS process.

The Cu_xO films were prepared by thermally oxidating the Cu layer on the Pt/Ti/SiO_2/Si substrate. Cu films were deposited using radio frequency (RF) reactive magnetron sputtering from a Cu target after standard cleaning of the substrate had been done. The as-prepared samples were ex-situ annealed in a high-purity oxygen ambient at 600 ℃ for 30 min. The top electrodes (molybdenum, Mo) were ex-situ sputtered onto the deposited thin films following a standard lithography process. Peaks identified as CuO and Cu_2O could clearly be observed (not shown here) from our x-ray diffraction study.

Fig. 7 (a) shows the current of an M-Cu_xO-M heterostructure versus the applied pulse cycles. Bistable on/off switching characteristics were obtained by applying a Set-V of 0.9 V for 10 μs and a Reset-V of -0.7 V for 30 μs. The resistance values were read at 0.2 V. A current switching window (more than one order) between the ON and OFF states was observed. Figure 7 (b) shows the resistance-changing ratio ($\Delta R/R_0=(R-R_0)/R_0$, R_0: the initial resistance value and R: the changed resistance value) of the ON state varied from -0.1 to 0.1, which indicates good distribution characteristics. Moreover, a resistance-changing ratio for the OFF state that varied from 20 to 80 was observed.

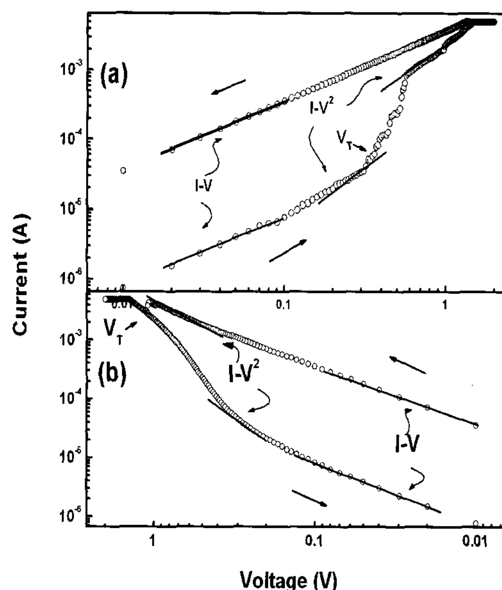

Fig. 8. I-V characteristics of M-Cu_xO-M heterostructures at 300 K in double-logarithmic plot: (a) Positive-bias and (b) negative-bias regions. Note that absolute values of current and voltage have been taken for both ordinates. Arrows indicate sweeping directions.

The switching mechanism of Cu_xO has been explained in detail in the following section. Cu_xO is regarded as a p-type semiconductor; therefore, the *I-V* characteristics of Cu_xO are mainly determined by the injection and transport of hole carriers. Figures 8 (a) show the logarithmic plots of *I-V* curves for positive-voltage regions and 8 (b) show those of negative regions. The *I-V* characteristics in the low-voltage region (Fig. 8 (a)) exhibit $I \propto V$ correlation (ohmic), followed by $I \propto V^2$. That can be explained by the effect of SCLC.[9] Thus, when the density of thermally generated free carriers inside the Cu_xO films is greater than that of injected charge carriers, $I \propto V$ correlations (ohmic behaviors) are observed. Once the injected excess carriers dominate the thermally generated carriers, carrier conduction is controlled by the shallow traps (the first $I \propto V^2$) given by

$$J = \frac{9\varepsilon_r \varepsilon_0 \mu V^2}{8L^3}\left(\frac{N_c}{N_t}\right)e^{\frac{-E}{kT}} , \quad (1)$$

where ε_r is the static dielectric constant, ε_0 is the permittivity of free space, and μ is the hole mobility. Here, V is the applied voltage, L is the film thickness, and N_c is the effective density of states in the valence band. The N_t is the number of shallow traps, E is the effective trapping potential, and T is the temperature. With further increases in the applied bias, the rate of rise in the current increases as voltage increases and obeys Child's law (the second $I \propto V^2$).

The fabrication of M-Cu_xO-M heterostructures was fully compatible with the standard CMOS process, and reproducible resistive switching was observed with a low switching voltage. The trapping (de-trapping) of SCLC contributed to the carrier transport (resistance) of M-Cu_xO-M heterostructures. Good retention characteristics can be obtained in M-Cu_xO-M heterostructures by accurately controlling the preparation parameters.

2. Resistive Switching of Cu:MoO_3

The resistive switching of Cu-doped MoO_x thin film, which is based on the formation and rupturing of multi-filaments, demonstrated uniform resistance and good data-retention characteristics. Cu-doped MoO_x films (~400 nm) were deposited on a Cu substrate at 500°C using a sputtering system with a 0.5 % Cu-doped MoO_3 target. The Pt top electrodes were formed using conventional photolithography. Fig. 9 plots typical *I-V* characteristics on a semi-logarithmic scale where large hysteresis can be observed at low voltages for both forward- and reverse-bias regions.

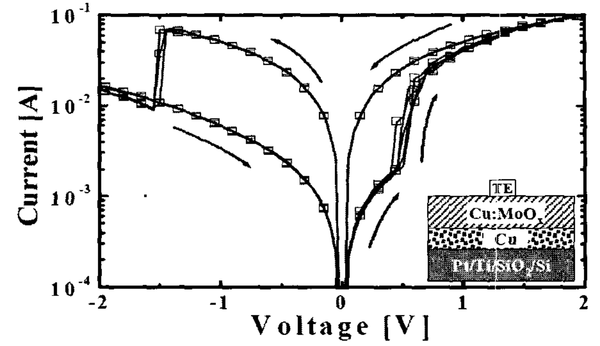

Fig. 9. Typical *I-V* characteristics of Pt/Cu:MoO_x/Cu devices.

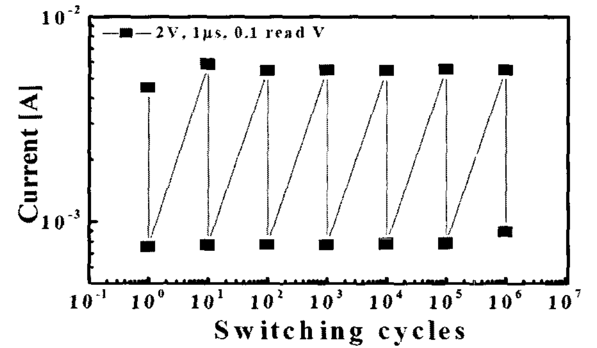

Fig. 10. Endurance data of Cu:MoO_x film for 10^6 cycles by applying voltage pulses.

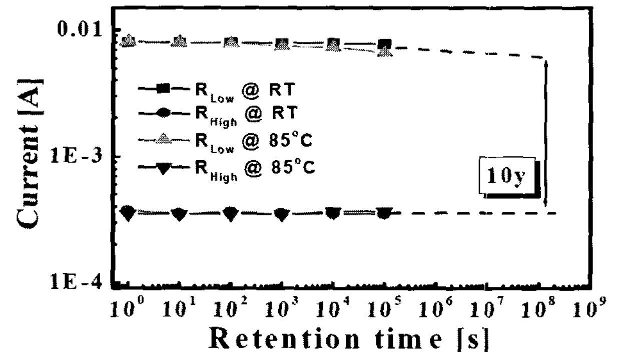

Fig. 11. Retention properties of R_{on} and R_{off} at room temperature and also at 85°C.

Fig. 10 plots the endurance characteristics under a voltage pulse of 2 V for 1 μs. HRS and LRS can be maintained under a cycle stress of up to 10^6 cycles. Fig. 11 also shows good data retention at 85 ℃, based on

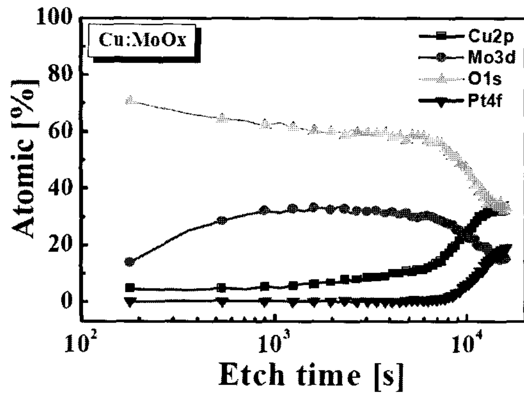

Fig. 12. XPS depth profiling of Cu:MoO$_x$ film deposited at 500°C. Cu is easily diffused into film.

extrapolation; the HRS and LRS can be retained for more than a decade.

XPS was carried out to clarify the physical mechanism responsible for resistance switching. Fig. 12 plots the XPS depth profiles for all elements of the films. Although a 0.5 % Cu-doped MoO_3 target was used, the atomic concentration of copper in the films was more than 5 %. The high Cu concentration in the bulk MoO$_x$ can be explained by thermal diffusion from the bottom Cu electrode during sputtering at 500℃.

Spreading-resistance images of the film surface were examined to observe microscopic behaviors involved in resistive switching. Fig. 13 shows the local conductance with a sufficient spatial resolution obtained by AFM (C-AFM). The peaks indicate localized high-conductance spots (LRS state). Once the HRS had formed, the conductive peaks were more spread out and had low intensity. This observation is consistent with the dependence of Cu-doped MoO$_x$ film on area in both states. The current levels were also reduced in HRS when the area of the top electrodes was scaled down. However, the LRSs were independent of area due to filamentary conduction. The resistive-switching behaviors of heavily Cu-doped molybdenum oxide can be explained based on these findings.

Since the conducting paths of copper can be generated by their formation process, high current can flow through conducting filaments in the ON state. The conducting filaments at opposite bias should be disconnected near the anode side through electrochemical reactions. Thus, the neutral copper in the matrix can be anodized into copper ions near the anode, which in turn disconnects the filaments.

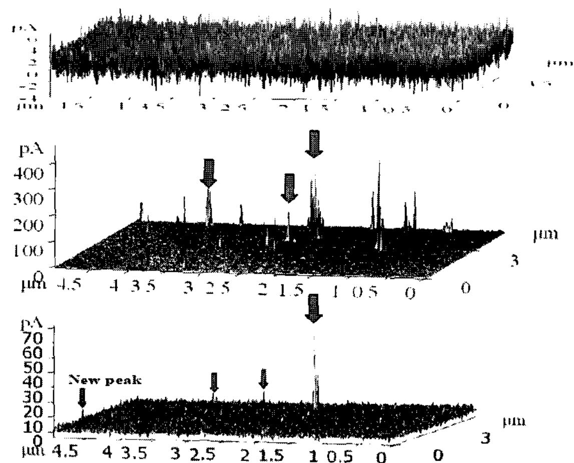

Fig. 13. Generation and rupturing of multi-filaments under applied voltage as recorded by spreading resistance image (SPI) of C-AFM.

We investigated the resistive switching of heavily Cu-doped MoO$_x$ thin film. A model was proposed based on the formation and rupturing of multi-filaments, and this was confirmed by AFM. Heavily Cu-doped MoO$_x$ shows promise for future NVM applications considering its superior resistive-switching behaviors and device uniformity.

3. Resistive Switching of $La_{0.7}Ca_{0.3}MnO_3$ Oxide

$Re_{1-x}A_xMnO_3$ materials have been extensively investigated for their numerous magnetoresistance properties, which have been confirmed from their remarkably rich phase diagrams as functions of temperature, magnetic field, and doping. We focused on the resistive-switching properties of $La_{0.7}Ca_{0.3}MnO_3$ (LCMO) perovskite oxide in this study and on improvements to electrical properties accomplished by post-deposition O_2 annealing.

The LCMO films were prepared using an RF sputtering system from an LCMO target onto a $Pt/Ti/SiO_2/Si$ substrate. The deposition temperature was 650°C, whereas the oxygen content was varied by controlling the $Ar:O_2$ ratio. The ratio was 20:0 sccm for sample 1 (S1) and 20:4.0 sccm for S2. Sample 3 was prepared with additional O_2 annealing of sample S2 at 650°C for 30 minutes.

Fig. 14 has the *I-V* plots on a semi-logarithmic scale for all three samples. A small hysteresis window was observed for sample S1 (Fig 14 (a)) that disappeared

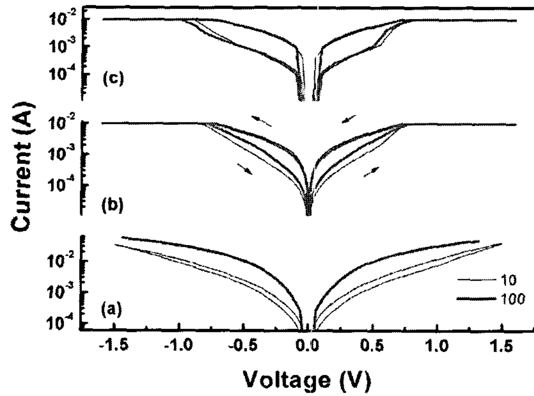

Fig. 14. Continuous *I-V* characteristics of Mo-LCMO-Pt structure under different preparation conditions.

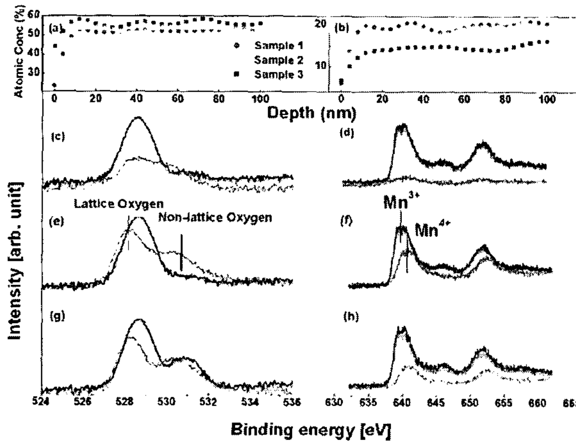

Fig. 15. XPS characteristics of LCMO film for S1, S2, and S3. (a) plots depth profile of atomic concentration of oxygen and (b) plots that of manganese. (c), (e), and (g) show depth profiles of O1s peaks that were measured on LCMO surface (thin line) and "bulk" with depths of 10 nm (moderate line) and 20 nm (thick line). (d),(f), and (h) show depth profiles of Mn 2p peaks that were measured on LCMO surface (thin line) and bulk with depths of 10 nm (moderate line) and 20 nm (thick line).

after 100 cycles. S2 had a larger window but also disappeared after consecutive sweeping cycles. S3, on the other hand, not only had the largest resistive window but it also retained a similar window even after being swept for 100 cycles.

The XPS data (Fig. 15) for Samples S1, S2, and S3 show increases in oxygen content in the sequence S3>S2>S1, consistent with the method the samples were prepared with. From the O1s peak in Fig. 15 (c) (S1), 2 (e) (S2), and 2 (g) (S3), only a single peak (528.1 eV) was observed for S1 which was in correlation with the lattice oxygen bonding in LCMO film; for S2, an additional peak (530.2 eV) was observed in the surface area. In contrast, both peaks were observed in the bulk and surface region for S3. The Mn^{4+}/Mn^{3+} had a strong dependence on the oxygen content. A chemical shift (641.3 to 639.6 eV) was observed in sample S2, which supports the earlier observation of the O1s peak.

Although the dominant operating mechanism is not yet clear, the fact that oxygen content is crucial for resistance switching has been well documented. The interactions between non-lattice site (mobile) oxygen and oxygen vacancies and/or cationic vacancies contribute to the carrier transport (resistance) of M-LCMO-M heterostructures. Good retention characteristics were obtained for these heterostructures by accurately controlling the preparation parameters.

IV. Resistive Switching of Single Crystal and Epitaxial Samples

1. Resistive Switching of Single Crystal Nb:STO

Single crystal Nb:STO (NbSTO) substrates not only demonstrate excellent resistance-switching behaviors but also provide the opportunity for explaining their switching mechanism. The surfaces of a single-crystal Nb (0.5 wt%): STO (100) substrate were ultrasonically degreased in a trichloroethylene (TCE), acetone, and methanol solution, and rinsed in DI water for 10 min. Pt was used as both the top and bottom electrodes. Figure 16 plots the hysteretic *I-V* characteristics of Pt/Nb:STO and Ti/Nb:STO junctions. The deep-work-function metal (Pt) contact has numerous hysteric *I-V* characteristics, whereas the shallow-work-function metal (Ti) exhibits ohmic behavior.

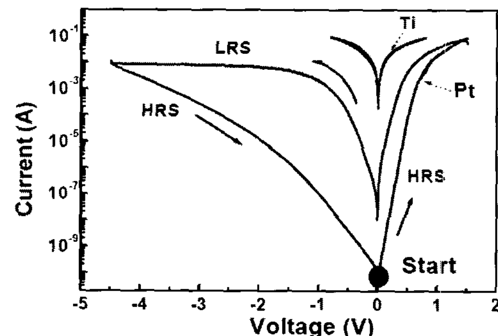

Fig. 16. Hysteresis *I-V* characteristics of Pt and Ti electrode on Nb:STO substrate.

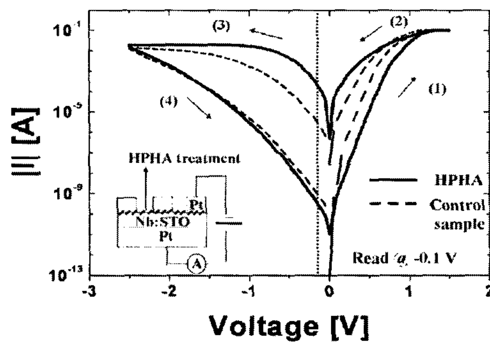

Fig. 17. *I-V* characteristics of control sample (dashed line) and HPHA sample (solid line). Inset shows device structure and configuration for measurement.

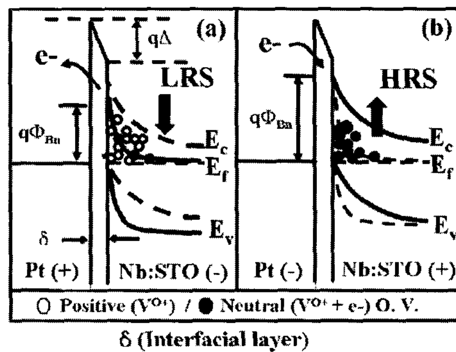

Fig. 18. (a) Schematic of Pt/Nb:STO Schottky junction based on intermediate region (δ) and voltage drop (Δ) through it. Net plus charge (V^{o+}) makes bandwidth/height narrower/lower, which creates LRS. (b) Large number of electrons is accumulated at interface states, which modify band barrier width/height and create HRS.

Fig. 17 plots Nb:STO switching after high-pressure hydrogen treatment (HPHA). A possible model for switching was proposed based on the modulation of tunneling barrier width by electron charging and discharging at an oxygen vacancy (V_o) in the depletion region, as seen in Fig. 18. This means that the applied positive-gate bias generates a positive charge (V^+_o) in the depletion region, and reduces the tunneling width, thus enabling LRS to be observed. In applied negative-gate bias, electron injection, which is from the top gate, will recombine with an oxygen vacancy (V^+_o), resulting in HRS.

The excellent uniformity and reproducibility of the resistance-switching characteristics of a Pt/single crystal Nb:STO Schottky junction have been reported. The switching characteristics were improved by treating the surfaces of Nb:STO substrates differently. Based on excellent memory properties such as long-term high-temperature stability, excellent uniformity, and exceptional reproducibility, Pt/Nb:STO Schottky-junction devices are very promising for future gigabit NVM applications.

2. Resistive Switching of Epitaxial Nb:STO

The literature has reported that perovskite oxides have good resistance switching on single-crystal oxide substrates such as $SrTiO_3$ and $LaAlO_3$ wafers. Single-crystal oxides have excellent reproducibility and uniformity, which is the main concern in polycrystalline films. However, it is very difficult to introduce single-crystal-perovskite oxides into the current silicon complementary metal oxide semiconductor (CMOS) process. The heteroepitaxial growth of perovskite oxides on Si substrates is necessary to introduce perovskite oxides into the CMOS process and preserve the switching characteristics of single-crystal films.

A buffer layer is necessary to grow epitaxial oxide on Si. We introduced a TiN buffer layer to grow epitaxial Nb:STO on a silicon substrate in this study. The TiN and Nb:STO films were grown with multi-target pulsed laser deposition (PLD) at a substrate temperature of 800^0C in a vacuum (~10^{-6} Torr). A laser beam was focused to obtain an energy density of 11 J/cm^2 with a repetition rate of 4 Hz to prepare the TiN films, and the energy density of the laser beam was 1.5 J/cm^2 and its repetition rate was 2 Hz for the Nb:STO films. An additional control Nb:STO film was prepared without a TiN buffer layer for comparison.

An Nb:STO film was deposited without a buffer layer on Si (100) at a substrate temperature of 800 ^{0}C in a vacuum as a control sample. Figure 19 (a) shows the XRD patterns of Nb:STO film, and the four peaks of Nb:STO (110), (111), (200), and (211) indicate that the Nb:STO film was polycrystalline. We observed (*h* 0 0) peaks for the Nb:STO film with a TiN buffer layer (Fig. 19 (b)), and a (2 0 0) peak for the TiN film; no other diffraction peaks that may have resulted from impurity phases or randomly oriented grains were observed. This means that the Nb:STO film had a textured structure with a cubic phase. The results further suggested that the crystal quality of the Nb:STO films deposited onto Si substrates was improved using TiN as a buffer layer.

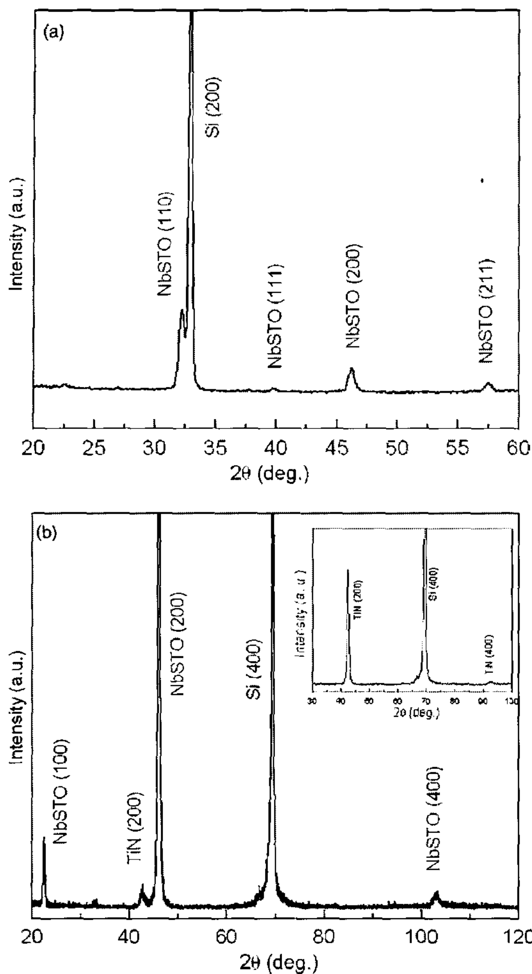

Fig. 19. XRD patterns of (a) Nb:STO film grown directly onto Si at 800°C in vacuum, and (b) Nb:STO film deposited at 800°C in vacuum on TiN/Si structure. Inset shows XRD pattern of TiN film deposited onto Si substrate.

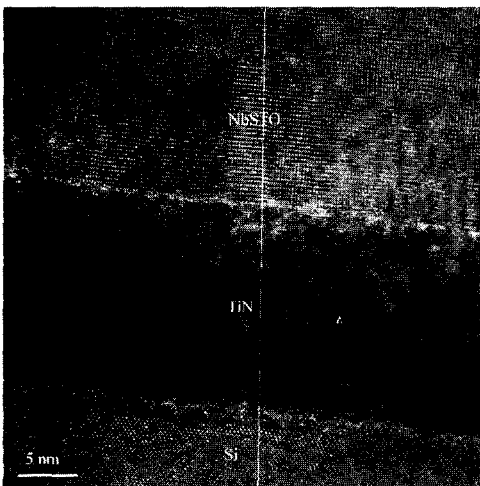

Fig. 20. HRTEM micrograph from Nb:STO/TiN/Si structure prepared at 800°C in vacuum. Sharp interfaces between Nb:STO/TiN and TiN/Si were observed.

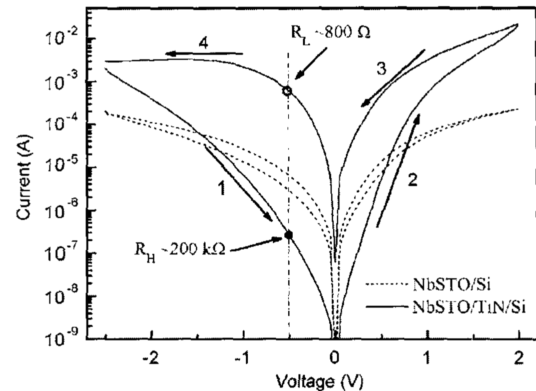

Fig. 21. Hysteretic *I-V* characteristics of Pt/Nb:STO/Si (open) and Pt/Nb:STO/TiN/Si structures (solid).

We also examined the film structure using a high-resolution TEM image. Fig. 20 shows an HRTEM image along <011> Si. The TEM image clearly demonstrates that TiN and Nb:STO films were epitaxially grown on silicon, although the films contained a high density of dislocations. Moreover, the Nb:STO/TiN and TiN/Si interfaces were found to be very smooth and free of any perceptible inter-mixing, indicating that the TiN buffer layer was a good barrier preventing interaction between the Nb:STO and Si substrate.

Fig. 21 plots the *I-V* characteristics of Nb:STO/Si and Nb:STO/TiN/Si structures, which are plotted on a semi-logarithmic current scale. As can be seen, the Nb:STO film with the TiN buffer layer has a higher resistance ratio than the control sample, which may have resulted from the improved crystal quality of the Nb:STO film and/or from the interface quality between the Pt electrode and epitaxial Nb:STO films.

The retention characteristics of a device measured at room temperature are shown in Fig. 22. The high- and low-resistance states remained unchanged over a period of 10^5 sec. The device-to-device uniformity was compared between epitaxial Nb:STO and other polycrystalline oxides as shown in Fig. 23.

Epitaxial Nb:STO films were grown on Si substrates using TiN as a buffer layer. The hysteresis in the *I-V* characteristics of the Nb:STO/TiN/Si samples was larger than that of the control sample without a TiN buffer layer. Stable write/erase operations were observed up to 10^4 cycles. The heteroepitaxial growth of perovskite oxides on Si exemplifies the promising potential of perovskite-oxide-based nonvolatile resistance memories.

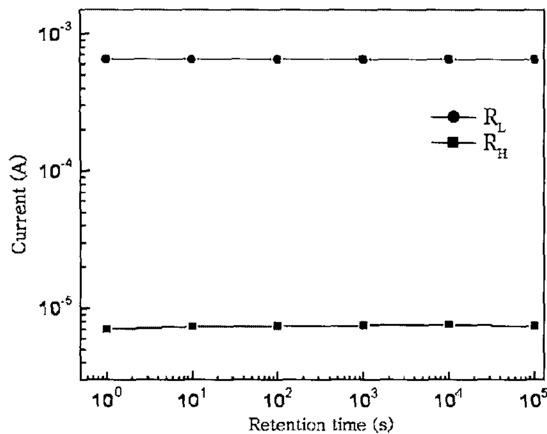

Fig. 22. Excellent retention of data was obtained at room temperature.

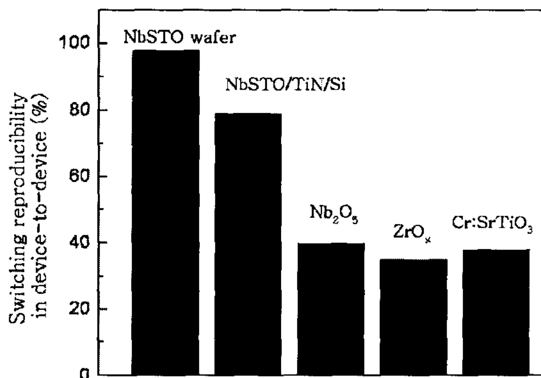

Fig. 23. Switching reproducibility of single-crystal Nb:STO wafer, Nb:STO/TiN/Si structure, and other polycrystalline oxides previously mentioned.

V. SUMMARY

In summary, the electrical characteristics of various binary oxides (e.g., Nb_2O_5, ZrO_x, Cu:MoO_x, and Cu_xO) and ternary oxides (e.g., Nb:STO) were investigated for ReRAM applications. Stoichiometric and/or non-stoichiometric polycrystalline oxides, which can be prepared by controlling deposition conditions, were evaluated. An MIS capacitor structure (Pt/ZrO_x/p-Si) based on ZrO_x clearly had two distinct memory states. Resistance (R) switching from one state to another can be attained by applying proper bias, and the mechanism of R switching can be explained by charge trapping. The R ratio between HRS and LRS in Nb_2O_5 films ranged from 50 to 100. Moreover, a retention test revealed that the memory lifetime was longer than a decade. ReRAM devices based on copper oxides are attractive propositions, considering their compatibility with the standard CMOS process. Both the trapping (de-trapping) of SCLC and the formation (deformation) of multi-filaments can explain resistance (R) switching. Good R switching and retention characteristics can be obtained by optimizing processes. A model was proposed based on the formation and rupturing of multi-filaments, which was confirmed by AFM, for the R-switching of heavily Cu-doped MoO_x thin film,.

Excellent uniformity and reproducibility of a Pt/single-crystal Nb:STO Schottky junction was reported for ternary oxides. Furthermore, heteroepitaxial growth of Nb:STO on Si substrates was carried out to introduce single-crystal perovskite oxides into the current CMOS process and preserve their switching characteristics, in which TiN was used as a buffer layer. The hysteresis in the *I-V* characteristics of the Nb:STO/TiN/Si samples was larger than that of the control sample without a TiN buffer layer and stable write/erase operations were observed up to 10^4 cycles.

Various problems such as switching uniformity, understanding of the switching mechanism, and process compatibility with current Si CMOSs need to be solved taking NVM applications into consideration. One solution to improving device uniformity is to use a single-crystalline matrix such as single-crystalline Nb:STO. Device uniformity was drastically improved compared to polycrystalline oxides. However, various problems such as process-complexity issues and slow-switching speed still need to be solved.

ACKNOWLEDGMENTS

This work was supported by "The National Research Program for 0.1 Terabit Non-Volatile Memory Development Sponsored by the Korean Ministry of Commerce, Industry and Energy" and the "Brain Korea 21 (BK21) Project".

REFERENCES

[1] International Technology Roadmap for Semiconductors (ITRS, 2006), http://www.itrs.net/reports.html.

[2] S. Q. Liu, N. J. Wu, and A. Ignatiev, *Appl. Phys. Lett.*, 76, 2749 (2000).

[3] A. Beck, J. G. Bednorz, C. Gerber, Ch. Rossel,

and D. Widmer, *Appl. Phys. Lett.,* 77, 139 (2000); S. Seo, M. J. Lee, D. H. Seo, E. J. Jeoung, D. S. Suh, Y. S. Joung, I. K. Yoo, I. R. Hwang, S. H. Kim, I. S. Byun, J. S. Kim, J. S. Choi, and B. H. Park, *Appl. Phys. Lett.,* 85, 5655 (2004).

[4] W. W. Zhuang, W. Pan, B. D. Ulrich, J. J. Lee, L. Stecker, A. Burmaster, D. R. Evans, S. T. Hsu, M. Tajiri, A. Shimaoka, K.Inoue, T. Naka, N. Awaya, K. Sakiyama, Y. Wang, S. Q. Liu, N. J. Wu, and A. Ignatiev, *IEDM Tech. Dig.,* p.193 (2002).

[5] A. Baikalov, Y. Q. Wang, B. Shen, B. Lorenz, S. Tsui, Y. Y. Sun, Y. Y. Xue, and C. W. Chu, *Appl. Phys. Lett.,* 83, 957 (2003).

[6] Y. Tokunaga, Y. Kaneko, J. P. He, T. Arima, A. Sawa, T. Fujii, M. Kawasaki, and Y. Tokura, *Appl. Phys. Lett.,* 88, 223507 (2004); Y. Kozuka, T. Susaki, and H. Y. Hwang, *Appl. Phys. Lett.,* 88, 142111 (2006).

[7] M. J. Rozenberg, I. H. Inoue, and M. J. Sánchez, *Phys. Rev. Lett.,* 92, 178302 (2004).

[8] A. Sawa, T. Fujii, M. Kawasaki, and Y. Tokura, *Appl. Phys. Lett.,* 85, 4073 (2004).

[9] T. Fujii, M. Kawasaki, A. Sawa, H. Akoh, Y. Kawazoe, and Y. Tokura, *Appl. Phys. Lett.,* 86, 012107 (2004).

[10] A. Odagawa, H. Sato, I. H. Inoue, H. Akoh, M. Kawasaki, Y. Tokura, T. Kanno, and H. Adachi, *Phys. Rev. B* 70, 224403 (2004).

[11] T. Oka and N. Nagaosa, *Phys. Rev. Lett.,* 95, 266403 (2005).

[12] A. Chen, S. Haddad, Y. C. Wu, T. N. Fang, Z. D. Lan, S. Avanzino, S. Pangrle, M. Buynoski, M. Rathor, W. Cai, N. Tripsas, C. Bill, M. VanBuskirk, and M. Taguchi, *IEDM Tech. Dig.,* p. 765 (2005).

[13] K. Szot, W. Speier, G. Bihlmayer, and R. Waser, *Nat. Mater.* 5,312 (2006).

[14] D. H. Choi, D. S. Lee, H. J. Sim, M. Chang, and H. S. Hwang, *Appl. Phys. Lett.* 88, 082904 (2006).

[15] D. S. Lee, H. J. Choi, H. J. Sim, D. H. Choi, H. S. Hwang, M. J. Lee, S. Seo, and I. K. Yoo, *IEEE Elec. Dev. Lett.,* 26, 719 (2005).

[16] R. Dong, Q. Wang, L. D. Chen, D. S. Shang, T. L. Chen, X. M. Li, and W. Q Zhang, *Appl. Phys. Lett.,* 86, 172107 (2005).

[17] H. J. Sim, H. J. Choi, D. S. Lee, M. Chang, D. H. Choi, Y. N. Son, E. H. Lee, W. J. Kim, Y. D. Park, I. K. Yoo, and H. S. Hwang, *IEDM Tech. Dig.,* p. 587 (2005).

[18] D. S. Lee, D. J. Seong, H. J. Choi, I. H. Jo, R. Dong, W. F. Xiang, S. J. Oh, S. H. Heo, M. S. Jo, D. K. Hwang, H. K. Park, M. Chang, M. Hasan, and H. S. Hwang, *IEDM Tech. Dig.,* p. 797 (2006).

[19] S. T. Hsu, T. K. Li, and N. Awaya, *J. Appl. Phys.,* 101, 024517 (2007).

[20] A. L. S. Loke, C. Ryu, C. P. Yue, J. S. H. Cho, and S. S. Wong, *IEEE Elec. Dev. Lett.,* 17, 549 (1996).

[21] J. D. McBrayer, R. M. Swanson, and T. W. Sigmon, *J. Electrochem. Soc.,* 133, 1242 (1986).

[22] N. Wakiya, N. Tajiri, T. Kiguchi, N. Mizutani, J. Cross, and K. Shinozaki, *Jap. J. of Appl. Phys.,* 45, 8827 (2006).

[23] S. Muraoka, K. Osano, Y. Kanzawa, S. Mitani, S. Fuji, K. Katayama, et al., *IEEE Elec. Dev. Meet.* 2007, pp. 779–782.

[24] M. Janousch, G. I. Meijer, U. Staub, B. Delley, S. F. Karg, and B. P. Andreasson, *Adv. Mater.* 19, 2232 (2007).

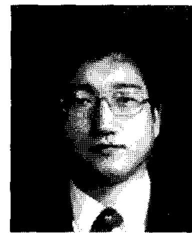

Hyunsang Hwang received the B.S. degree in metallurgical engineering from Seoul National University, Seoul, Korea, in 1988, and the Ph.D. degree in materials science from the University of Texas at Austin in 1992. From 1992 to 1997, he was with the LG Semicon Co., Korea, as a Principal Researcher. In 1997, he joined the faculty at Gwangju Institute of Science and Technology, Gwangju, Korea, as a Professor in the Department of Materials Science and Engineering. He is working on nonvolatile memory devices including ReRAM and SONOS, high-k gate dielectric and ultra shallow junction. He has published more than 150 papers in international journals.

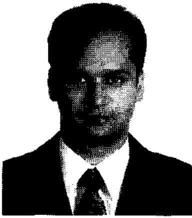

Musarrat Hasan received his B.Sc. Engineering degree from Bangladesh University of Science and Technology (BUET) in 2002 and M.Sc. from Catholic university, Leuven (KULeuven) of Belgium in 2003. He is currently pursuing his Ph.D. degree is Materials Science and Engineering at Gwangju Institute of Science and Engineering (GIST). His current work involved metal gate electrode and high-k gate dielectric application for CMOS technology and resistance random access memory device for future non-volatile memory application. He is author and co-author of few SCI journals

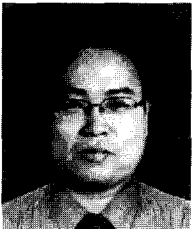

Rui Dong received the B.S. degree in applied chemistry from Zhengzhou University in 1998. He received his M.S. degrees in physical chemistry from East China Normal University (Shanghai) in 2002. His Ph.D degree in materials science and engineering was received from Shanghai Institute of Ceramics (Chinese Academy of Sciences) in 2005. He has a "Brain of Korea for 21th century" (BK21) postdoctoral research fellowship at Gwangju Institute of Science & Technology (GIST) from 2005 to present.
He has worked in the research of semiconductor device physics and in the development of process integration of the next generation non-volatile memory (NVM) product. His current research interests include the design, fabrication and physical mechanism of Resistance Random Access Memory (Re-RAM). He has authored and co-authored over 30 research papers and currently holds several China patents.

Dongsoo Lee received a B.S. degree in Ceramic Engineering from Yonsei University in 2002, and a M.S. degree in Materials Science Engineering from Gwangju Institute of Science and Technology in 2004, and present as a Ph. D candidate at GIST.
His current research interest is Resistance Random Access Memory (RRAM) applications.

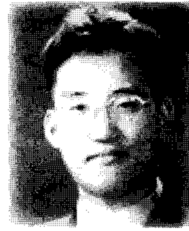

Dong-jun Seong received a B.S. and M.S. degree in Chemical Engineering from Yonsei University in 2000, 2002, respectively. He joined Semiconductor Integrated Device and Process Lab., GIST in 2005 and present as a Ph. D candidate at same place. His current research interest is Resistance Random Access Memory (RRAM) applications.

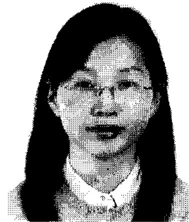

Hye jung Choi received the B.S. degree in Materials Science Engineering from Pusan National University, Busan, Korea in 2003 and the M.S. degrees in Materials Science Engineering from Gwangju Institute of Science and Technology, Gwangju, Korea in 2004. where she is currently pursuing the Ph.D. degree in materials science and engineering. Her current research interests are design, scaling and modeling of nonvolatile memory devices such as ReRAM and Nanocrystal memory.

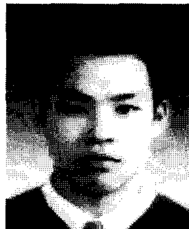

Myeongbum Pyun received the B.S. degree in Chemical Engineering from Inha University, Incheon, Korea in 2006.and He currently pursuing the M.S. degrees in Materials Science Engineering from Gwangju Institute of Science and Technology, Gwangju. His current research interests are design, scaling and modeling of nonvolatile memory devices such as Resistive Random Access Memory (ReRAM).